NOMA-assisted UWVLC System for Terrestrial-to-Underwater AUV Networks

Nikhil Sharma
Electronics and Communication Engg.
The LNMIIT
Jaipur, India
nikhil.sharma@lnmiit.ac.in

Divyang Rawal
Electronics and Communication Engg.
The LNMIIT
Jaipur, India
divyang.rawal@lnmiit.ac.in

Hardik Soni
Nav Wireless Technologies Pvt Ltd
Ahmedabad
Gujarat, India
hardik.soni@navtechno.in

Abstract—The connectivity of autonomous underwater vehicles (AUV) with the ground station (GS) plays a significant role in oceanic exploration and monitoring. Therefore, non-orthogonal multiple access (NOMA) assisted efficient cooperative system model connecting the terrestrial base station (TBS) with the AUVs via a floating vessel (FV). It guarantees robust and reliable data delivery from the GS to the AUV nodes. The proposed system caters to the underwater demands for high data rate communication. The paper explores the feasibility of a dual-hop system for connecting multiple AUVs to the TBS. While data from the TBS to FV is transmitted over a radio frequency (RF) carrier, the low latency underwater visible light communication (UWVLC) network connects the AUVs to the FV. Decode-and-forward relay is deployed at the FV, which acts as an interface between terrestrial and underwater communication. The RF link is modelled by the Nakagami-m distribution, whereas the UWVLC link is characterized by the Exponential Generalized Gamma (EGG) distribution. Exact closed-form expressions of average BER are derived for underwater NOMA users. Numerical results depict the effect of aquatic parameters such as air bubbles, temperature gradient and salinity level on the system performance.

Index Terms—Exponential Generalized Gamma distribution, Nakagami-m fading, Non-orthogonal multiple access, underwater visible light communication.

I. INTRODUCTION

A reliable and robust underwater (UW) communication mode is necessary to envisage the new UW activity. In the recent past, there has been an increase in the research on UW sensor networks and unmanned UW vehicles, which have numerous applications such as tactical surveillance, oil field exploration, disaster prevention, oceanic monitoring, data collection, and autopilot operations [1], [2]. The potential candidates for UW wireless communication are acoustic, radio frequency (RF) and optical wireless communication [3]. On the other hand, the complex UW environment affects the RF-assisted UW link and increases hardware expenditure and its limited use in shallow water bodies. To combat the detrimental effects of acoustic and RF waves, an attractive alternative to UW communication is UW visible light communication (UWVLC) link [3], [4]. The UWVLC link operates with negligible latency and offers a potentially high bandwidth transmission to support a data rate in Mbps/Gbps.

In the last decade, a trend has been followed to increase the transmission distance and data rate of the UWVLC system. It is observed that the laser-based UWVLC system provides a much larger bandwidth and high data rate as compared to the LED-based UWVLC system. The researchers in [5] achieved the data rate of 7.2 Gbps over a transmission distance of 6 m using blue lasers. Furthermore, several studies have been conducted to model turbulence in UW scenarios. Authors in [6] utilized the log-normal distribution to model the irradiance fluctuations due to oceanic turbulence. The authors evaluated the closed-form expression of end-to-end bit error rate (BER) for multi-hop UW optical wireless communication in [7]. In [2], [8], a unified statistical model in the form of Exponential Generalized Gamma (EGG) distribution is proposed to model the turbulence-induced fading in UWVLC links. This channel model perfectly fits the experimental data by considering air bubbles and temperature gradients with fresh and salty waters.

In addition, NOMA-assisted UW wireless communication caters to many devices in the UW scenario [9], [10]. The distinguishing feature of NOMA is to support many users with the help of non-orthogonal resource allocation. However, limited studies have been carried out for NOMA-aided UW wireless communication. Moreover, most of these works are based on the analysis of multi-user UW acoustic communication [11]. Authors in [12] analyzed the performance of a full-duplex (FD) relay-assisted UW acoustic network with the NOMA approach. It is observed that the considered relay-assisted system experiences a higher sum rate as compared to the direct link system, irrespective of the interference cancellation efficiency. The authors in [13] propose a photon-counting receiver for NOMA UW optical wireless communication system. Further, authors in [14] presented the analytical expressions of the coverage probability and cell capacity for weak UW turbulence in the NOMA-aided UWVLC system. In [15], a NOMA-assisted UWVLC system to connect multiple AUVs is presented. However, it lacks the link connecting the FV to the ground station (GS). The standalone FV can provide limited data to the AUVs and thus require a continuous update from the GS regarding weather conditions and instructions to the AUVs.

Motivated by the above observations, we propose a relay-assisted NOMA UWVLC system in which the RF link from the TBS is relayed at the FV and retransmitted using the NOMA scheme. We have shown the effect of various wa-

ter qualities on system performance. The proposed system may adopt in naval services as the integration of NOMA with UWVLC has led to improved spectrum efficiency, more connections and lower latency. The original contributions of this work are as follows. (i) We derive the novel closed-form expression of end-to-end BER for the considered dual-hop RF-UWVLC system in the presence of successive interference cancellation (SIC) errors for strong and weak users. (ii) We have validated the derived closed-from expressions for the considered system with the numerical results. (iii) The results depict the feasibility of the proposed system for both fresh and salty water ecosystems.

The remaining paper is organized as follows: The detailed description of the system model and the transmission protocol is demonstrated in Section II. Section III describes the channel models used for the RF and UWVLC links. Section IV presents the performance analysis regarding average BER for considered NOMA-assisted asymmetric RF/UWVLC system. Numerical results for various UW scenarios are presented in Section V followed by the conclusion given in Section VI.

II. System Model

The proposed system model is presented in Fig. 1. It consists of a terrestrial GS, FV and two AUVs classified as strong and weak NOMA end users depending on the channel conditions. This model fits well to the application for transmitting vital information from the GS to the AUV, including coordinates, direction and various system settings for a mission-critical application. A GS may serve multiple AUVs available via FV at different depths and channel conditions. Hence, the NOMA downlink is used to efficiently utilize the limited power available at the FVs. The complex UW ecosystem shows channel impairments such as varying bubble levels, turbulence and salinity. The EGG channel model is used to characterize the effects of all the channel impairments. The AUV with better channel condition is referred to as strong AUV (AUV_s) and the other one as weak AUV (AUV_w). The end-to-end transmission from GS to AUVs occurs in two-time phases. In the first phase, GS transmits information to the FV using the RF carriers subjected to Nakagami-m fading. The signal received at FV is given as

$$y_{fv} = h_{s,fv}x + n_{s,fv}, \tag{1}$$

where $h_{s,fv}$ is the channel coefficient of Nakagami-m distributed GS-FV link, $n_{s,fv}$ is the additive white Gaussian noise (AWGN) with zero mean and variance $\sigma_I^2 = \frac{N_o}{2}$, i.e., $n_{s,fv} \sim \mathcal{N}(0, \sigma_I^2)$. The signal x is transmitted with power P_s from GS to FV. x is assumed to be a fourth-order pulse amplitude modulated (4-PAM) constellation whose signal space representation is shown in Fig. 2. The constellation points $x \in \{x_s, x_w\}$ consists of two bits where x_s represents the information bit for strong AUV (AUV_s) and x_w represents the information bit for weak AUV (AUV_w). In phase II, the DF relay available at FV decodes the received signal y_{fv} and transmits it to the UW optical carriers. The detected information symbols at FV are scaled appropriately as r_s and
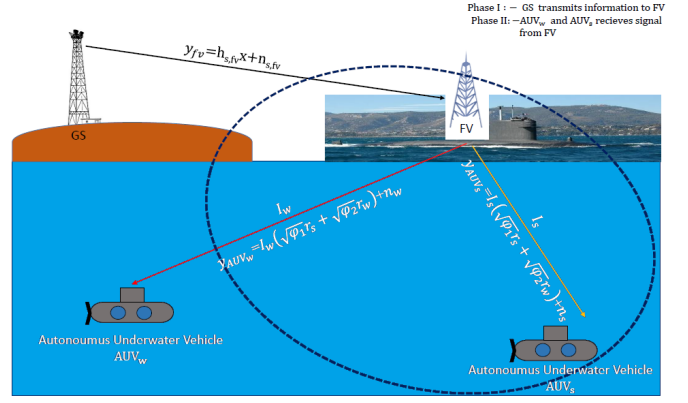
Fig. 1: DL-NOMA Assisted RF/UWVLC based System

r_w, which are further combined by employing superposition coding (SC) and transmitted to AUV_s. The SC symbol is further transmitted to the AUVs. Let P_t represent the power transmitted by the FV. The received signal at the AUV_s and AUV_w is expressed as

$$y_{AUV_i} = \eta I_i \hat{r}_{sc} + n_i, \text{where } i = \{s, w\} \tag{2}$$

where η is the responsivity i.e., optical to electrical conversion coefficient, I_i indicates the real-valued irradiance fluctuations of the corresponding link modeled by EGG distribution and n_i is the AWGN with zero mean and variance $\sigma_I^2 = \frac{N_o}{2}$, i.e., $n_i \sim \mathcal{N}(0, \sigma_I^2)$. $\hat{r}_{sc} = \sqrt{\varphi_1}r_s + \sqrt{\varphi_2}r_w$ is the SC symbol which is on-off keying (OOK) modulated, where $\varphi_1 = \beta_s P_s$ is the power allocated to AUV_s and $\varphi_2 = \beta_w P_s$ is the power allocated to AUV_w, $\beta_s = \delta$, $\beta_w = (1 - \delta)$ and δ denotes the power allocation coefficient. At weak AUV, maximum likelihood (ML) detection is employed to decode its own symbol r_w treating r_s as interference. The SIC mechanism is applied at strong AUV, and the desired information is obtained by sequential demodulation and decoding. It is assumed that the channel gain of strong AUV is greater than that of weak AUV, i.e., $|I_s|^2 > |I_w|^2$. Thus a higher power level is normally allocated to AUV_w. The r_w is detected directly using ML detection at AUV_w considering r_s as interference. At AUV_s, firstly r_w is detected first which further eliminated from y_{AUV_s} to decode the symbol r_s.

III. Channel Model

This section explains the channel model considered for characterizing the RF and the UWVLC link. Nakagami-m and EGG distribution depict the RF and UWVLC link channel, respectively, considering the effect of salinity, temperature gradient, and air bubbles.

A. Terrestrial Ground Station-FV Link

To model the GS-FV link, we have considered Nakagami-m distribution whose probability density function (PDF) [16, Eq.(5.14)], is given as

$$f_{\rho_{s,fv}}(\rho) = \frac{m^m \rho^{m-1}}{\bar{\rho}_{RF}^m \Gamma(m)} \exp\left(\frac{-m\rho}{\bar{\rho}_{RF}}\right), \tag{3}$$
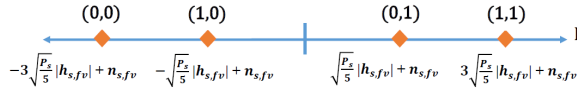
Fig. 2: Signal Constellation of 4-PAM
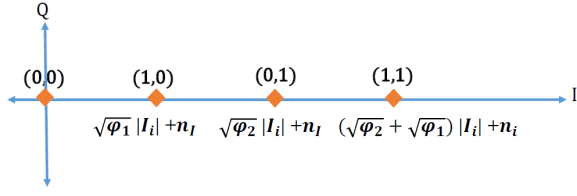
Fig. 3: SC OOK signal received by NOMA Users, $\{i = s, w\}$

where m depicts the shaping parameter, ranges from 0.5 to ∞, $m = 1$ approximates the PDF to that of the Rayleigh distribution (special case). ρ represents the signal to noise ratio (SNR), $\bar{\rho}_{RF}$ is the average SNR of RF link, and $\Gamma(\cdot)$ is the Gamma function.

B. Underwater Visible Light Communication (UWVLC) Link

The UWVLC link is assumed to be EGG distributed, which considers the detrimental effects of air bubbles, oceanic turbulence and the salinity of the water. The variation in the parameters of EGG distribution for the temperature gradient and thermally uniform temperature are shown in [8]. It is observed that the EGG channel distribution is modelled as the weighted sum of the exponential and the generalized Gamma distributed channels, given in [8] as

$$f_I(I) = \omega_o f(I; \lambda_o) + (1 - \omega_o) g(I; [a_o, b_o, c_o]), \quad (4)$$

$$f(I; \lambda_o) = \frac{1}{\lambda_o} \exp\left(-\frac{I}{\lambda_o}\right)$$

$$g(I; [a_o, b_o, c_o]) = c \frac{I^{a_o c_o - 1} \exp\left(-\left(\frac{I}{a_o}\right)^c\right)}{b_o^{a_o c_o} \Gamma(a_o)}, \quad (5)$$

where g presents the generalized Gamma distribution, f denotes exponential distribution and , ω_o denotes the mixture coefficient, where, $0 < \omega_o < 1$, λ_o represents the scale parameter of exponential distribution, while a_o, b_o and c_o are the parameters representing generalized Gamma distribution and $\Gamma(\cdot)$ denotes the Gamma function. The instantaneous signal-to-noise ratio (SNR) is analytically represented based on the detection techniques, i.e., intensity modulation/direct detection (IM/DD) or heterodyne detection (HD) as

$$\rho_{UWVLC} = \frac{(\eta I)^r}{N_o}, \quad (6)$$

where r denotes the detection type,i.e., $r = 1$ and $r = 2$ corresponds to the HD and IM/DD detection, respectively. Further, the average SNR of UWVLC link, can be written as

$$\bar{\rho}_{UWVLC} = \frac{\mu_r \mathbb{E}[I^r]}{\mathbb{E}[I]^r}, \quad (7)$$

where $\mu_r = (\eta \mathbb{E}[I])^r / N_o{}^1$ is the function of the average electrical SNR. The unified expression of PDF of UWVLC link i.e., EGG distributed channel in terms of SNR is expressed as given in [8] as

$$f_{\rho_{fv,uv}}(\rho) = \frac{\omega_o}{r\rho} G_{0,1}^{1,0}\left[\frac{1}{\lambda_o}\left(\frac{\rho}{\mu_r}\right)^{\frac{1}{r}}\middle| \begin{array}{c} - \\ 1 \end{array}\right]$$
$$+ \frac{c(1-\omega_o)}{r\rho \Gamma(a_o)} G_{0,1}^{1,0}\left[\frac{1}{b_o^{c_o}}\left(\frac{\rho}{\mu_r}\right)^{\frac{c_o}{r}}\middle| \begin{array}{c} - \\ a_o, b_o \end{array}\right], \quad (8)$$

where $G_{p,q}^{m,n}\left(x\middle| \begin{array}{c} a_1, \ldots, a_p \\ b_1, \ldots, b_q \end{array}\right)$ is the Mejier's G function. The average electrical SNR $\mu_r = \mu_1 = \bar{\rho}_{UWVLC}$ for HD whereas $\mu_r = \mu_2$ for IM/DD technique is given as

$$\mu_2 = \frac{\bar{\rho}_{UWVLC}}{2\omega_o \lambda_o^2 + b_o^2(1-\omega_o)\Gamma(a_o + 2/c_o)/\Gamma(a_o)}. \quad (9)$$

Further, it is also observed that the exponential Gamma (EG) fading channel model can be derived as a special case of EGG fading model by assuming uniform temperature and substituting $c = 1$ in (8).

IV. PERFORMANCE ANALYSIS

In this section, we analyze the performance of the considered NOMA-assisted RF-UWVLC system in the presence of imperfect SIC scenario. In particular, this paper derives novel closed-form expressions of the average BER for the UW vehicles AUV_s and AUV_w.

A. Average BER Analysis

A 4-PAM modulated signal is received over the GS-FV link in the first time phase. The signal space representation of the same is illustrated in Fig. 2. Further, constellation points of the received signal are decoded to retrieve the information bits for the AUVs. In the second time phase, the information bits of the AUVs are SC and transmitted to both AUV_s and AUV_w using the OOK modulation scheme. The constellation diagram of the same is shown in Fig. 3. To derive the end-to-end average BER of the proposed system, the individual link's (GS-FV, FV-AUV_i) average BER are computed in the following subsections.

1) BER Analysis at Floating Vessel($\bar{P}_e^{GS-FV}$): The instantaneous BER of 4-PAM signal received by FV can be written as given in [17] as

$$P_e^{GS-FV} = \frac{3}{2}Q\left(\sqrt{\rho_{RF}}\right), \quad (10)$$

where $\rho_{RF} = \frac{2}{5}\frac{P_s}{N_o}|h_{s,fv}|^2$. Further, the average BER is obtained by averaging the above expression over PDF of Nakagami-m fading as

$$\bar{P}_e^{GS-FV} = \frac{3}{2}\int_0^\infty Q\left(\sqrt{\frac{2P_s}{5N_o}|h_{s,fv}|^2}\right) f_{\rho_{s,fv}}(\rho)\,d\rho. \quad (11)$$

Expressing (11) in terms of moment generating function (MGF) of Nakagami-m as given in [16, Eq.(5.15)] and further

---

$^1\mathbb{E}$ is the expectation operator and $\mathbb{E}[I^r]$ represents the r$^{\text{th}}$ moment of I.

solving the integral, the expression for average BER is given as

$$\bar{P}_e^{GS-FV} = \frac{3}{4\sqrt{\pi}} \frac{\Gamma\left(m+\frac{1}{2}\right)}{\Gamma(m+1)} \times \frac{\sqrt{\bar{\rho}_{RF}/2m}}{(1+\bar{\rho}_{RF}/2m)^{m+(1/2)}}$$
$$\times \, {}_2F_1\left(1, m+\frac{1}{2}, m+1, \frac{2m}{2m+\bar{\rho}_{RF}}\right), \quad (12)$$

where m is an non-integer value and $\bar{\rho}_{RF} = \mathbb{E}\{\rho_{RF}\}$.
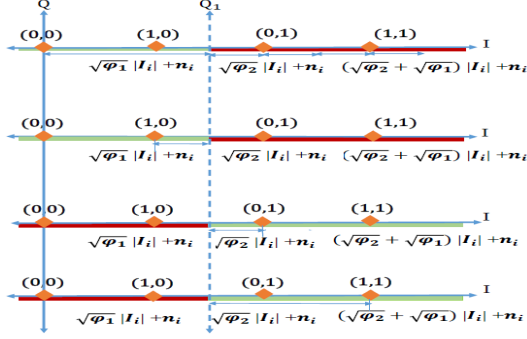
Fig. 4: Signal Constellation of NOMA weak User AUV_w.

2) BER Analysis at Weak User $(\bar{P}_e^{GS-AUV_w})$: The signal space constellation of the received signal at the users AUV_s and AUV_w during phase II is shown in Fig. 3. The signal constellation for user AUV_s and AUV_w are represented by the binary bits of strong and weak users, i.e., (r_s, r_w), that belongs to OOK signalling. The Green line depicts the correct decision region, while the red line depicts the region of erroneous decoding. The decision boundary for weak NOMA user AUV_w as observed from the Fig. 4 is Q_1. For the constellation point $\{0,0\}$, the weak user bit $r_w = 0$ is erroneously detected as $r_w = 1$ in the right side of decision axis Q_1. Similarly, for the symbol $\{1,0\}$, the erroneous region lies to the right side of the decision axis Q_1. Further, if we analyse the constellation point $\{0,1\}$, error occurs when $r_w = 1$ is erroneously detected as $r_w = 0$ which occurs in the region to the left side of decision axis Q_1. Similarly, the weak user bit $r_w = 1$ of symbol $\{1,1\}$ is detected erroneously in the interval $[Q \ Q_1]$.

ML detection process is applied at (AUV_w) to decode r_w from the received SC symbol. Assuming all the signal constellation points are equiprobable with prior probability $\frac{1}{4}$. The PDF corresponding to the constellation point $(0,0)$ can be expressed as $f_{(0,0)} = \frac{1}{\sqrt{2\pi\sigma^2}}e^{\frac{-(x-0)^2}{2\sigma^2}}$. Thus the error probability for the constellation point $(0,0)$ can be expressed as $P_{AUV_{w|(0,0)}} = \int_{\sqrt{\frac{\rho_1}{2}}}^{\infty} e^{\frac{-(x-0)^2}{N_o}} dx = \mathcal{Q}\left(\sqrt{\rho_1}\right)$, where $\mathcal{Q}(\cdot)$ denotes the Gaussian $\mathcal{Q}$-function and $\rho_1 = \frac{\bar{\rho}_{UWVLC}}{2}\left(\sqrt{\beta_w} + \sqrt{\beta_s}\right)^2|I_w|^2$. The composite instantaneous BER corresponding to the $FV - AUV_w$ connection may be calculated as a result of applying a similar mathematical technique to determine the BER corresponding to each individual constellation point.

$$P_{AUV_w} = \frac{1}{4}\left[2\mathcal{Q}\left(\sqrt{\rho_1}\right) + 2\mathcal{Q}\left(\sqrt{\rho_2}\right) - \mathcal{Q}\left(\sqrt{\rho_3}\right) - \mathcal{Q}\left(\sqrt{\rho_4}\right)\right].$$
$$(13)$$
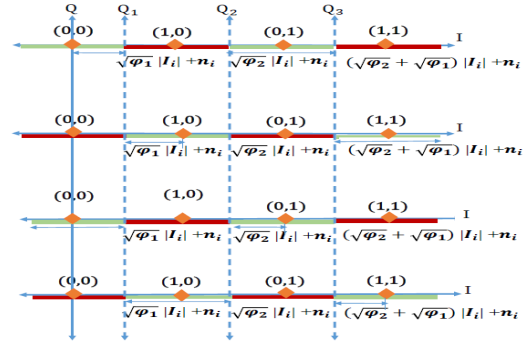
Fig. 5: Signal Constellation of NOMA strong User AUV_s.

where $\rho_2 = \frac{\bar{\rho}_{UWVLC}}{2}\left(\sqrt{\beta}_w - \sqrt{\beta}_s\right)^2|I_w|^2$, $\rho_3 = 2\bar{\rho}_{UWVLC}\beta_w|I_w|^2$ and $\rho_4 = 2\bar{\rho}_{UWVLC}\left(\sqrt{\beta}_w + \sqrt{\beta}_s\right)^2|I_w|^2$. Further, the average BER at weak user AUV_w is derived using (8) and (13) as

$$\bar{P}_e^{FV-AUV_w} = \frac{1}{4}\left[\underbrace{2\int_0^{\infty} \mathcal{Q}(\sqrt{\rho_1})f_{\rho_1}(\rho_1)\,d\rho_1}_{T_I} + \underbrace{2\int_0^{\infty}\mathcal{Q}(\sqrt{\rho_2})f_{\rho_2}(\rho_2)d\rho_2}_{T_{II}}\right.$$
$$\left.\underbrace{-\int_0^{\infty}\mathcal{Q}(\sqrt{\rho_3})f_{\rho_3}(\rho_3)d\rho_3}_{T_{III}} \underbrace{-\int_0^{\infty}\mathcal{Q}(\sqrt{\rho_4})f_{\rho_4}(\rho_4)d\rho_4}_{T_{IV}}\right], \quad (14)$$

Substituting the identities $\mathcal{Q}(x) = \frac{1}{2}erfc\left(\frac{x}{\sqrt{2}}\right)$, $erfc(\sqrt{x}) = \frac{1}{\sqrt{\pi}}G_{1,2}^{2,0}\left[x \left|\begin{matrix}1\\0,\frac{1}{2}\end{matrix}\right.\right]$ [18, Eq.(8.4.14/2)] and (8) in T_I of (14) , we get

$$T_I = \frac{1}{2\sqrt{\pi}}\int_0^{\infty}G_{1,2}^{2,0}\left[\frac{\rho_1}{2}\left|\begin{matrix}1\\0,\frac{1}{2}\end{matrix}\right.\right]\frac{\omega_o}{r\rho_1}G_{0,1}^{1,0}\left[\frac{1}{\lambda_o}\left(\frac{\rho_1}{\mu_r}\right)^{\frac{1}{r}}\left|\begin{matrix}-\\1\end{matrix}\right.\right]$$
$$+\frac{1}{2\sqrt{\pi}}\int_0^{\infty}G_{1,2}^{2,0}\left[\frac{\rho_1}{2}\left|\begin{matrix}1\\0,\frac{1}{2}\end{matrix}\right.\right]\frac{c_o(1-\omega_o)}{r\rho_1\Gamma(a_o)}G_{0,1}^{1,0}\left[\frac{1}{b_o^{c_o}}\left(\frac{\rho_1}{\mu_r}\right)^{\frac{c_o}{r}}\left|\begin{matrix}-\\a_o\end{matrix}\right.\right]. \quad (15)$$

For the ease of simplification, the Mejier's G function in (15) is substituted by its equivalent Fox-H function [18, Eq.(8.4.51/9)]. A modified expression is given as

$$T_I = \frac{\omega}{2\sqrt{\pi}r}\int_0^{\infty}\rho_1^{-1}H_{0,1}^{1,0}\left[\frac{1}{\lambda}\left(\frac{\rho_1}{\mu_r}\right)^{\frac{1}{r}}\left|\begin{matrix}-\\(1,1)\end{matrix}\right.\right]H_{1,2}^{2,0}\left[\frac{\rho_1}{2}\left|\begin{matrix}(1,1)\\(0,1),(\frac{1}{2},1)\end{matrix}\right.\right]d\rho_1$$
$$+\frac{c_o(1-\omega_o)}{2\sqrt{\pi}r\Gamma(a_o)}\int_0^{\infty}\rho_1^{-1}H_{0,1}^{1,0}\left[\frac{1}{b_o^{c_o}}\left(\frac{\rho_1}{\mu_r}\right)^{\frac{c_o}{r}}\left|\begin{matrix}-\\(a_o,1)\end{matrix}\right.\right]$$
$$\times H_{1,2}^{2,0}\left[\frac{\rho_1}{2}\left|\begin{matrix}(1,1)\\(0,1),(\frac{1}{2},1)\end{matrix}\right.\right]d\rho_2. \quad (16)$$

Integral in (16) can be further simplified with the help of the identity given in [19, Eq.(2.8.4)] as

$$T_I = \frac{\omega_o}{2\sqrt{\pi}r}H_{2,2}^{1,2}\left[\frac{1}{\lambda_o}\left(\frac{2}{\mu_r}\right)^{\frac{1}{r}}\left|\begin{matrix}(1,\frac{1}{r}),(\frac{1}{2},\frac{1}{r})\\(1,1),(0,\frac{1}{r})\end{matrix}\right.\right]$$
$$+\frac{c_o(1-\omega_o)}{2\sqrt{\pi}r\Gamma(a_o)}H_{2,2}^{1,2}\left[\frac{1}{b_o^{c_o}}\left(\frac{2}{\mu_r}\right)^{\frac{c_o}{r}}\left|\begin{matrix}(1,\frac{c_o}{r}),(\frac{1}{2},\frac{c_o}{r})\\(a_o,1),(0,\frac{c_o}{r})\end{matrix}\right.\right]. \quad (17)$$

Further, utilizing the identity $H_{p,q}^{m,n} \left[z \left| \begin{array}{c} (a_i, \alpha_i)_{1,p} \\ (b_j, \beta_j)_{1,q} \end{array} \right. \right] = k H_{p,q}^{m,n} \left[z^k \left| \begin{array}{c} (a_i, k\alpha_i)_{1,p} \\ (b_j, k\beta_j)_{1,q} \end{array} \right. \right]$ as given in [19, Eq.(2.1.4)], the T_I of the average BER at NOMA weak user can be further simplified as

$$T_I = \frac{\omega_o}{2\sqrt{\pi}} H_{2,2}^{1,2} \left[\frac{2}{\lambda_o^r \mu_r} \left| \begin{array}{c} (1,1), \left(\frac{1}{2}, 1\right) \\ (1,r), (0,1) \end{array} \right. \right]$$
$$+ \frac{(1-\omega_o)}{2\sqrt{\pi}\Gamma(a_o)} H_{2,2}^{1,2} \left[\frac{2}{b_o^r \mu_r} \left| \begin{array}{c} (1,1), \left(\frac{1}{2}, 1\right) \\ \left(a_o, \frac{r}{c_o}\right), (0,1) \end{array} \right. \right]. \quad (18)$$

Similarly, by applying the same process we can solve the integrals for T_{II} to T_{IV}. The closed-form expression of average BER at weak user (AUV_w) as shown in (19) is obtained after substituting the simplified expressions of T_I to T_{IV} in (14).

$$\bar{P}_e^{FV-AUV_w} = \frac{1}{4} \left[2\mathbb{X}(\bar{\rho}_1) + 2\mathbb{X}(\bar{\rho}_2) - \mathbb{X}(\bar{\rho}_3) - \mathbb{X}(\bar{\rho}_4) \right], \quad (19)$$

where $\mathbb{X}(\bar{\rho}_j) = \frac{\omega_o}{2\sqrt{\pi}} H_{2,2}^{1,2} \left[\frac{2}{\lambda^r \mu_r} \left| \begin{array}{c} (1,1), \left(\frac{1}{2}, 1\right) \\ (1,r), (0,1) \end{array} \right. \right] +$ $\frac{(1-\omega_o)}{2\sqrt{\pi}\Gamma(a_o)} H_{2,2}^{1,2} \left[\frac{2}{b_o^r \mu_r} \left| (1,1), \left(\frac{1}{2},1\right), \left(a_o, \frac{r}{c_o}\right), (0,1) \right. \right], \mu_r = \frac{\bar{\rho}_j}{2\omega_o \lambda_o^2 + b_o^2(1-\omega_o)\Gamma(a_o+2/c)/\Gamma(a_o)}, \bar{\rho}_j = E\{\rho_j\}, j\epsilon\{1,2,3,4\}$ for NOMA weak user.

3) BER Analysis at Strong User ($\bar{P}_e^{GS-AUV_s}$): The decision boundary corresponding to the strong user (AUV_s) for computing its BER is determined using Q_1, Q_2 and Q_3 axis as shown in Fig. 5. It is clearly observed from Fig. 5 that for the constellation points $\{0,0\}$ and $\{0,1\}$ an error is said to occur when the first bit $\{r_s\}$ is erroneous i.e., 0→1. Thus, erroneous symbol is either $\{1,0\}$ or $\{1,1\}$, thus the error boundaries will be $[Q_1 \ Q_2]$ and to the right of Q_3. Similarly, for the symbols $\{1,0\}$ and $\{1,1\}$, the erroneous symbols will be $\{0,0\}$ and $\{0,1\}$ and the error boundaries will be $[Q_2 \ Q_3]$ and to the left of Q_1. It is observed that the error region on the right of the axis Q_3 for a point $\{0,0\}$ and the region $[Q_2, Q_3]$ for point $\{1,0\}$ is due to the NOMA error propagation (error incurred during detection of a weak user (AUV_w) bits) resulting from the decoding error of a strong user (AUV_s).

The instantaneous BER at strong user is obtained by the summation of individual error probabilities corresponding to each constellation point multiplied by its prior probability and is given as

$$P_{AUV_s} = \frac{1}{4} \left[\mathcal{Q}(\sqrt{\rho_5}) + 3\mathcal{Q}(\sqrt{\rho_6}) - \mathcal{Q}(\sqrt{\rho_7}) + 2\mathcal{Q}(\sqrt{\rho_8}) \right.$$
$$\left. - 2\mathcal{Q}(\sqrt{\rho_9}) + \mathcal{Q}(\sqrt{\rho_{10}}) - \mathcal{Q}(\sqrt{\rho_{11}}) - \mathcal{Q}(\sqrt{\rho_{12}}) \right], \quad (20)$$

where $\rho_5 = \frac{\bar{\rho}_{UWVLC}}{2} \left(-\sqrt{\beta_w} + \sqrt{\beta_s}\right)^2 |I_s|^2, \rho_6 = \frac{\bar{\rho}_{UWVLC}\beta_s |I_s|^2}{2}, \rho_7 = 2\bar{\rho}_{UWVLC}\beta_s |I_s|^2, \rho_8 = \frac{\bar{\rho}_{UWVLC}}{2} \left(\sqrt{\beta_w} - \sqrt{\beta_s}\right)^2 |I_s|^2, \rho_9 =$

$\frac{\bar{\rho}_{UWVLC}}{2} \left(\sqrt{\beta_w} - \sqrt{\beta_s}\right)^2 |I_s|^2, \rho_{10} = \frac{\bar{\rho}_{UWVLC}}{2} \left(\sqrt{\beta_w} + \sqrt{\beta_s}\right)^2 |I_s|^2, \rho_{11} = 2\bar{\rho}_{UWVLC} \left(\sqrt{\beta_w} - \sqrt{\beta_s}\right)^2 |I_s|^2, \rho_{12} = \frac{\bar{\rho}_{UWVLC}}{2} \left(\sqrt{\beta_w} + \sqrt{\beta_s}\right)^2 |I_s|^2$.

Further, the average BER at strong user AUV_s can be derived by adopting a similar mathematical procedure used to derive the average BER at the weak user. The closed-form expression of average BER at the strong user is shown in (21).

$$\bar{P}_e^{FV-AUV_s} = \frac{1}{4} \left[\mathbb{X}(\bar{\rho}_5) + 3\mathbb{X}(\bar{\rho}_6) - \mathbb{X}(\bar{\rho}_7) + 2\mathbb{X}(\bar{\rho}_8) \right.$$
$$\left. - 2\mathbb{X}(\bar{\rho}_9) + \mathbb{X}(\bar{\rho}_{10}) - \mathbb{X}(\bar{\rho}_{11}) - \mathbb{X}(\bar{\rho}_{12}) \right], \quad (21)$$

where $\mathbb{X}(\bar{\rho}_j) = \frac{\omega_o}{2\sqrt{\pi}} H_{2,2}^{1,2} \left[\frac{2}{\lambda^r \mu_r} \left| \begin{array}{c} (1,1), \left(\frac{1}{2}, 1\right) \\ (1,r), (0,1) \end{array} \right. \right] +$ $\frac{(1-\omega_o)}{2\sqrt{\pi}\Gamma(a_o)} H_{2,2}^{1,2} \left[\frac{2}{b_o^r \mu_r} \left| (1,1), \left(\frac{1}{2},1\right), \left(a_o, \frac{r}{c_o}\right), (0,1) \right. \right], \mu_r = \frac{\bar{\rho}_j}{2\omega_o \lambda_o^2 + b_o^2(1-\omega_o)\Gamma(a_o+2/c)/\Gamma(a_o)}, \bar{\rho}_j = E\{\rho_j\}, j \in \{5,6,\ldots,12\}$ for NOMA strong user.

4) Average BER Analysis of End-to-End Link ($\bar{P}_e^{GS-AUV_i}$): Error at any of the AUV is said to occur if any of the two links (GS-FV and FV-AUV_i) are erroneous or both of the links are erroneous. Thus, the end-to-end BER at AUV_i, $i = s, w$ can be expressed as

$$\bar{P}_e^{GS-AUV_i} = \bar{P}_e^{GS-FV} + \bar{P}_e^{FV-AUV_i} - 2\bar{P}_e^{GS-FV} \times \bar{P}_e^{FV-AUV_i}, \quad (22)$$

Further, utilizing the derived expressions of average BER for GS-FV and $FV - AUV_i$ link in (22), we get the end-to-end average BER at NOMA strong and weak users $GS - AUV_i$.

V. NUMERICAL RESULTS AND DISCUSSIONS

In this section, numerical results are presented for the proposed NOMA-assisted DF-based RF-UWVLC system to cater needs of UW vehicles. The results are presented to get a graphical demonstration of the system behaviour for various system parameters. Values of various UW system parameters such as ω_o, λ_o, a_o, b_o and c_o are given in [8]. The same parameter (m) is assumed to be unity unless explicitly mentioned. The average channel variance for UW NOMA strong user AUV_s and weak user AUV_w are considered as $\mathbb{E}\left[|I_s|^2\right] = 0$dB and $\mathbb{E}\left[|I_w|^2\right] = -3$dB, respectively. In all the results, the $\bar{\rho}_{RF}$ is assumed to be 30dB.

The dependence of average BER on the bubble level and water salinity is demonstrated in Fig. 6. With the increase in saline level, the BER performance of the system degrades. Similarly, as the bubble level increases, the value of the scintillation index also rises, due to which BER deteriorates. It is interesting to note that the effect of BL is more dominant over the system performance than the effect of the salinity of the water. Another important observation from Fig. 6 is that before a cutoff SNR, the error performance of the strong user is poorer than that of the weak user despite the better channel conditions. It happens because, for lower SNR values, the weak user's transmitted power dominates over the channel conditions. Further, it is observed that beyond the cutoff SNR, the system behaves intuitively, i.e. the performance of the strong user becomes better than that of the weak user.
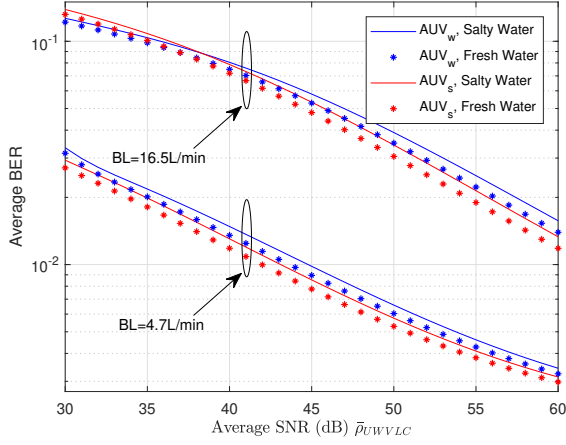
Fig. 6: BER versus $\bar{\rho}_{UWVLC}$ for varying salinity and BL
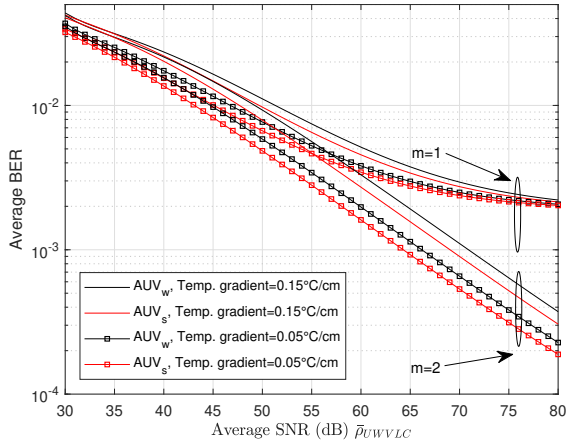
Fig. 7: BER versus $\bar{\rho}_{UWVLC}$ for different value of fading figure and temperature gradient

Fig. 7 demonstrates the variance of the average BER curve for a different temperature gradient keeping the bubble level constant at $2.4L/min$. It is observed that an increase in the temperature gradient leads to an increase in the average BER. It is because temperature rise increases the scintillation index and hence the higher UW turbulence. The shape parameter (m) of the Nakagami-m fading also plays its part in characterizing the system performance. It is observed that an increase in the value of m leads to a lower average BER due to the increased LOS component.

VI. Conclusion and Future Scope

This paper investigated the role of various performance metrics for NOMA-assisted DF-based RF-UWVLC systems in a downlink scenario. A new closed-form expression of the average BER is derived from a generalized Fox-H function for both NOMA users. Additionally, the system's performance is analyzed for different UW scenarios, such as bubble level, the salinity of water, and temperature gradient. This study assists the system designers in selecting parameters to suit their water ecosystem while maintaining performance. In future work, we extend this work with ergodic capacity analysis and optimal power allocation for salty and fresh water for more than two NOMA users over UWVLC systems.

References

[1] Z. Zeng, S. Fu, H. Zhang, Y. Dong, and J. Cheng, "A survey of underwater optical wireless communications," *IEEE Commun. Surveys Tuts.*, vol. 19, no. 1, pp. 204–238, 2017.

[2] E. Zedini, H. M. Oubei, A. Kammoun, M. Hamdi, B. S. Ooi, and M.-S. Alouini, "A new simple model for underwater wireless optical channels in the presence of air bubbles," in *IEEE Global Commun. Conf.*, pp. 1–6, 2017.

[3] N. Saeed, A. Celik, T. Y. Al-Naffouri, and M.-S. Alouini, "Underwater optical wireless communications, networking, and localization: A survey," *Ad Hoc Networks*, vol. 94, p. 101935, 2019.

[4] M. Jain, N. Sharma, A. Gupta, D. Rawal, and P. Garg, "Performance analysis of NOMA assisted underwater visible light communication system," *IEEE Wireless Commun. Lett.*, vol. 9, no. 8, pp. 1291–1294, 2020.

[5] T.-C. Wu, Y.-C. Chi, H.-Y. Wang, C.-T. Tsai, and G.-R. Lin, "Blue laser diode enables underwater communication at 12.4 gbps," *Scientific reports*, vol. 7, no. 1, pp. 1–10, 2017.

[6] H. Gerçekcioğlu, "Bit error rate of focused gaussian beams in weak oceanic turbulence," *JOSA A*, vol. 31, no. 9, pp. 1963–1968, 2014.

[7] M. V. Jamali, A. Chizari, and J. A. Salehi, "Performance analysis of multi-hop underwater wireless optical communication systems," *IEEE Photon. Technol. Lett.*, vol. 29, no. 5, pp. 462–465, 2017.

[8] E. Zedini, H. M. Oubei, A. Kammoun, M. Hamdi, B. S. Ooi, and M.-S. Alouini, "Unified statistical channel model for turbulence-induced fading in underwater wireless optical communication systems," *IEEE Trans. Commun.*, vol. 67, no. 4, pp. 2893–2907, 2019.

[9] M. Jain, S. Soni, N. Sharma, and D. Rawal, "Performance analysis at far and near user in NOMA based system in presence of sic error," *AEU-Int. J. Electron. Commun.*, vol. 114, p. 152993, 2020.

[10] S. M. R. Islam, N. Avazov, O. A. Dobre, and K.-s. Kwak, "Power-domain non-orthogonal multiple access (NOMA) in 5G systems: Potentials and challenges," *IEEE Commun. Surveys Tuts.*, vol. 19, no. 2, pp. 721–742, 2017.

[11] M. J. Bocus, D. Agrafiotis, and A. Doufexi, "Non-orthogonal multiple access (NOMA) for underwater acoustic communication," in *IEEE 88th Veh. Technol. Conf. (VTC-Fall)*, pp. 1–5, 2018.

[12] E. A. Makled, A. Yadav, O. A. Dobre, and R. D. Haynes, "Hierarchical full-duplex underwater acoustic network: A NOMA approach," in *OCEANS 2018 MTS/IEEE Charleston*, pp. 1–6, 2018.

[13] M. Li and Y. Xiang, "A photon counting underwater NOMA wireless optical communication system," in *7th Int. Conf. Inf., Commun. Netw. (ICICN)*, pp. 120–124, 2019.

[14] C. Geldard, J. Thompson, and W. O. Popoola, "A study of non-orthogonal multiple access in underwater visible light communication systems," in *IEEE 87th Veh. Technol. Conf.e (VTC Spring)*, pp. 1–6, 2018.

[15] A. Gupta, N. Sharma, P. Garg, D. N. K. Jayakody, C. Y. Aleksandrovich, and J. Li, "Asymmetric satellite-underwater visible light communication system for oceanic monitoring," *IEEE Access*, vol. 7, pp. 133342–133350, 2019.

[16] M. K. Simon and M.-S. Alouini, *Digital communication over fading channels*. New York: Wiley, 2001.

[17] J. R. Barry, E. A. Lee, and D. G. Messerschmitt, *Digital communication*. Springer Science & Business Media, 2012.

[18] A. P. Prudnikov, Y. A. Brychkov, O. I. Marichev, and R. H. Romer, "Integrals and series," 1988.

[19] A. A. Kilbas, *H-transforms: Theory and Applications*. CRC Press, 2004.